Indian Ocean Sea Surface Temperature and El Niño-Southern Oscillation: A New Perspective

Pascal Terray, Sébastien Dominiak

Indian Ocean Sea Surface Temperature and El Niño-Southern Oscillation: a new perspective

Pascal Terray [1,2] and Sébastien Dominiak[1]

[1] *Laboratoire d'Océanographie Dynamique et de Climatologie, IPSL, Paris, France*

[2] *Université Paris 7, Paris, France*

Submitted to Journal of Climate, July 2004

Revised October 2004

Corresponding author:

Pascal Terray

Laboratoire d'Océanographie Dynamique et de Climatologie, IPSL, Université Pierre et Marie Curie,

BP 100, 4 Place Jussieu, 75252 Paris CEDEX 05, France

Phone: (33) 1 44 27 70 78

Fax: (33) 1 44 27 38 05

email: terray@lodyc.jussieu.fr

Abstract

Here we show that the 1976-1977 climate regime shift was accompanied by a remarkable change in the lead-lag relationships between Indian Ocean Sea Surface Temperature (SST) and El Niño evolution. After the 1976-1977 regime shift, a correlation analysis suggests that southern Indian Ocean SSTs observed during late boreal winter are a key precursor in predicting El Niño evolution as the traditional oceanic heat content anomalies in the equatorial Pacific or zonal wind anomalies over the equatorial western Pacific. The possible physical mechanisms underlying this highly significant statistical relationship are discussed. After the 1976-1977 regime shift, southern Indian Ocean SST anomalies produced by Mascarene High pulses during boreal winter trigger coupled air-sea processes in the tropical eastern Indian Ocean during the following seasons. This produces a persistent remote forcing on the Pacific climate system, promoting wind anomalies over the western equatorial Pacific and modulating the regional Hadley cell in the southwest Pacific. These modulations, in turn, excite Rossby waves, which produce quasi-stationary circulation anomalies in the extratropical South Pacific, responsible for the development of the southern branch of the “horseshoe” El Niño pattern.

The change of the background SST state that occured in the late 1970s over the Indian Ocean may also explain why ENSO evolution is different before and after the 1976-1977 regime shift. These results shed some light on the possible influence of global warming or decadal fluctuations on El Niño evolution through changes in teleconnection patterns between the Indian and Pacific Oceans.

1. Introduction

A great deal of scientific research has focused on the existence of a climate shift in the Pacific Ocean basin in the mid-1970s (Nitta and Yamada, 1989; Trenberth and Hurell**,** 1994; Graham, 1994; Guilderson and Schrag, 1998). These inter-decadal climate fluctuations are characterized by a deeper-than-normal Aleutian Low pressure system, accompanied by negative SST anomalies in the north Pacific and enhanced westerly winds across the central North Pacific after 1977. Another key aspect of this Pacific Decadal Oscillation (PDO) is the significant warming in the central and eastern tropical Pacific Ocean and associated enhanced convective activity over the central Pacific since 1976-1977 (Nitta and Yamada, 1989; Nitta and Kachi, 1994; Wang, 1995; Kachi and Nitta, 1997). Thus, the spatial patterns of the PDO resemble those associated with El Niño in some aspects (Trenberth and Hurrell, 1994; Zhang et al., 1997; Garreaud and Battisti, 1999; Deser et al., 2004).

Meanwhile, several studies demonstrate that the evolution of ENSO is different before and after the 1976-1977 regime shift (Wang, 1995; An and Wang, 2000; Wang and An, 2001). The period, amplitude, spatial structure, and temporal evolution of El Niño events have significantly changed during recent decades. In addition, the ENSO-monsoon relationship has also weakened considerably after 1976-1977 (Kumar and Rajagopalan, 1999; Kinter et al., 2002). These changes in ENSO properties occurred concurrently with the Pacific decadal climate fluctuation. Clearly, the interdecadal

fluctuation in the North Pacific climate is linked to the interannual and interdecadal variations of the climate over tropical Indo-Pacific areas. However, the origins of both the decadal fluctuation and the tropical variations are a controversial matter in the scientific community.

The Indian Ocean also experienced a sudden surface warming around 1976-1977, suggesting an abrupt climatic change in these regions during recent decades (Nitta and Yamada, 1989; Terray, 1994; Aoki et al., 2003). The physical mechanisms for these changes are not yet fully understood and may be partly related to the PDO (Nitta and Yamada, 1989; Deser et al., 2004). The importance of secular variations in the Indian Ocean areas has been pointed out by Allan et al. (1995). They showed that the correlation structure of ENSO over the Indian Ocean has undergone secular variations in phase with the decadal changes in the Indian Ocean. This raises the important question of how the 1976-1977 Indian Ocean warming may influence the teleconnection patterns between the Indian and Pacific Oceans on the interannual time scale. This topic has been only marginally addressed in previous observational studies (Sewell and Landman, 2001; Trenberth et al., 2002). Thus, the primary goal of this study is to further investigate the Indian Ocean SST-ENSO relationships and describe their decadal variations, noting especially the changes that have taken place around the 1976-1977 regime shift, in order to re-examine the role of the Indian Ocean in ENSO dynamics. Here, we demonstrate through lagged correlation and regression analyses applied to new and improved SST and SLP datasets (Smith and Reynolds, 2002; Smith and Reynolds, 2004) that the 1976-1977 climate shift alters the lead-lag relationships between the Indian and Pacific Oceans. The observational results reported here strongly support the

hypothesis that the Indian Ocean now plays a fundamental role in the ENSO cycle (Yu et al., 2003; Wu and Kirtman, 2004).

The paper is organized as follows. Data and methods are briefly described in Section 2. Section 3 is devoted to a description of the lead-lag relationships between Indian Ocean SSTs and ENSO for time periods before and after the 1976-1977 regime shift. In Section 4, we examine in detail the physical mechanisms responsible for the highly significant relationship between boreal winter SST in the southeastern Indian Ocean and ENSO transitions observed during recent decades. In Section 5, we investigate the possible role of the abrupt changes in the SST background state over the Indian Ocean around 1976-1977 on the relationship between Indian Ocean SSTs and ENSO on the interannual time scale. Concluding remarks are given in Section 6.

2. Observations and statistical techniques

A large variety of datasets are used in this study to assess the Indian Ocean-ENSO relationships and their decadal variations. The SST dataset is the version 2 of the Extended Reconstruction of global SST (ERSST) developed on a 2° X 2° grid by Smith and Reynolds (2004). This analysis uses sea-ice concentrations to improve the high-latitude SST reconstruction and advanced statistical methods. However, similar results are obtained with version1 of the ERSST dataset (Smith and Reynolds, 2003), the Global sea Ice and Sea Surface Temperature (GISST) or the Hadley Centre sea Ice and Sea Surface Temperature (HadISST1) datasets compiled by the United Kingdom Meteorological Office Hadley Centre (Rayner et al., 2003). Thus, our results are largely independent of the SST dataset used in the computations. The Sea Level Pressure (SLP) dataset used here is the new Extended Reconstruction of oceanic Sea-Level Pressure

(ERSLP) analysis based on the Comprehensive Ocean-Atmosphere Data Set (COADS) and station data derived recently by Smith and Reynolds (2002). This SLP dataset includes data up to the year 1997. The different wind time series used in this study are computed from the latest version of the COADS, with updates through 1997 (Woodruff et al., 1998). Upper ocean monthly data are from the University of Maryland Simple Ocean Data Assimilation (SODA; Carton et al., 2000). The depth of the main thermocline (estimated using the depth of the 20°C isotherm) used in Section 3 is computed from the SODA product. Finally, we also use rainfall data from the gridded Climate prediction center Merged Analysis of Precipitation (CMAP) dataset (Xie and Arkin, 1997) and the National Center for Environmental Prediction-National Center for Atmospheric Research (NCEP-NCAR) reanalysis outputs (Kalnay et al., 1996) in order to document the air-sea interactions in the Indo-Pacific areas during recent decades, after the 1976-1977 regime shift.

Spatial and temporal characteristics of the Indo-Pacific climate variability are examined through standard lead-lag cross-correlations and regressions techniques and, Singular Value Decomposition (SVD) analysis for various atmospheric and oceanic fields. For a tutorial on SVD, the reader is referred to Bretherton et al. (1992) and Zhang et al. (1998). To account for the effects of autocorrelation, the statistical significance of the correlations and regressions coefficients has been assessed with a phase-scrambling bootstrap test (Davison and Hinkley, 1997). This statistical test takes directly into account the autocorrelation characteristics of the time series for assessing the confidence level of the correlations. A similar technique has been illustrated by Ebisuzaki (1997) in the climate literature. The correlation and regression maps shown in this paper are masked (or shaded) to exhibit only correlations that exceed the 90%

confidence level estimated by this bootstrap procedure with 999 samples (Davison and Hinkley, 1997).

In Section 3, the statistical significance of the difference of the observed correlations before and after the 1976-1977 climate shift was estimated through the procedure in Noreen (1989), based on a permutation test with 9999 shuffles. In the description of Figure 1, correlations are emphasized if they are significantly different from the 1948-1976 to 1977-2001 periods at the 90% level according to this permutation test.

3. Indian Ocean SSTs and the ENSO cycle

In order to determine the Indian and Pacific Oceans SST variability that is related to an ENSO event, and to describe the decadal variations of this relationship with special reference to the 1976-1977 climate shift, we correlate 2-month average SST fields with the December-January mean Niño3.4 (5°S-5°N/170°-120°W) SST time series, an indicator of ENSO variability. The correlations are calculated beginning one year prior to the Niño3.4 SST, separately for the two periods 1948-1976 and 1977-2001 (Fig. 1). The SST dataset used in these computations is the ERSST dataset. In what follows, we emphasize only those features that are significant at least at the 90% confidence level and that differ significantly from the pre- to post-1976-1977 correlation fields (see Section 2).

Figure 1 confirms that ENSO behaves differently before and after the 1976-1977 regime shift. First, striking and well-known changes are observed in the tropical Pacific during the onset and development phases of El Niño events between the two periods

(Wang, 1995; Zhang et al., 1997). Before the 1976-1977 regime shift, a canonical ENSO is exhibited, with a westward propagation of anomalous SSTs from the South American coast into the central equatorial Pacific during the development phase of El Niño (Wallace et al., 1998). After the shift, anomalous SSTs are first seen in the central equatorial Pacific, then propagate eastward to reach the South American coast several months later (Wang, 1995). During the mature phase of El Niño events, the pre- and post-1976-1977 correlation fields display the traditional "horseshoe" pattern characteristic of ENSO. However, the negative correlations forming the two branches of the "horseshoe" pattern are more intense after 1976.

Another key aspect of the decadal fluctuation is the notable difference in the evolution of Indian Ocean SST anomalies associated with ENSO for the pre- and post-1976-1977 periods (Fig. 1). Before the 1976-1977 regime shift, significant positive correlations first appear over the North Arabian Sea during the late Indian summer monsoon (August-September, Fig. 1d). These positive correlations expand southward and eastward during the following seasons. During the mature phase of El Niño (La Niña) (December-January, Fig. 1f), the whole Indian Ocean is significantly warmer (colder). This suggests that the ENSO signal is initiated in the Pacific and is then propagated westward into the Indian Ocean through atmospheric teleconnections (Klein et al., 1999; Alexander et al., 2002).

This Indian Ocean SST evolution is consistent with the coherent and well-documented inverse relationship between Indian Summer Monsoon (ISM) rainfall and El Niño before the 1976-1977 regime shift (Webster et al., 1998). Weak (strong) ISMs typically occur during the development stage of El Niño (La Niña) (Wang et al., 2001;

Terray et al., 2003). A weak monsoon is followed by a large warm SST anomaly over the tropical Indian Ocean due to decreased Ekman transports, vertical mixing and evaporation associated with the weaker monsoon winds. This anomaly persists for several months after the end of the monsoon (Rao and Goswami, 1988; Terray, 1995; Babu and Joseph, 2002). The warm Indian Ocean SST anomaly first observed in August-September during ENSO development may be interpreted in this context.

Turning now to the post-1976-77 period, the association between the Pacific and Indian Oceans remains strong, but the slow evolution of Indian Ocean SST anomalies is strikingly different. After the 1976-1977 climate shift, El Niño onset is preceded by a basinwide cooling in the Indian Ocean (Fig. 1g). The cold SST anomalies are particularly high in the South East Indian Ocean (SEIO), off the Australia coast. The core of this cold anomaly decreases slightly in intensity and area, moving northward from off the Australian coast to off the Java coast during spring and summer, then off the Sumatra coast by October–November (Figs. 1h-k). From boreal spring to fall, the cold SEIO SST anomalies are also associated with the development of the southern branchs of the El Niño “horseshoe” pattern (Figs. 1h-k). Another important factor to be recognized is the emergence of a Tropical Indian Ocean Dipole (TIOD) SST pattern (Saji et al., 1999) over the tropical Indian Ocean by October-November of the El Niño year (Fig. 1k). The degree of dependency of TIOD on ENSO is currently a controversial matter in the scientific community (Allan et al., 2001; Yamagata et al., 2002). However, all of these features are absent during the developing phase of El Niño prior to 1976. A slight warming of the tropical Indian Ocean is finally observed during the mature phase of El Niño after 1976. But, once again, this slight warming must be contrasted with the large and intense basinwide warming observed during the same season prior to 1976.

This differential warming of the Indian Ocean from the pre- to post-1976-77 regime shift periods is consistent with the weakening of the monsoon-ENSO relationship during recent decades (Kumar et al., 1999; Kinter et al., 2002).

Recent studies emphasize the passive role of the Indian Ocean in the development of ENSO (Wallace et al., 1998; Alexander et al., 2002). This seems to be true before the 1976-1977 regime shift, but not after (Fig. 1). The evolution of Indian Ocean SSTs during the initiation and development of ENSO and its change over time around the 1976-1977 regime shift, illustrated in Figure 1, suggest that the Indian Ocean may play an active role in the transition phases of ENSO after 1977. This possibility should not be overlooked (Yu et al., 2003). In particular, the SEIO area in boreal winter emerges as a key precursor of ENSO evolution after the 1976-1977 regime shift. In order to illustrate this, Figure 2 presents a systematic exploration of lead relationships in the initiation and development phases of ENSO through a time sequence of lagged correlations between the monthly Niño3.4 SST index and various ENSO predictors, including the SEIO SST anomaly in boreal winter, for both the pre- and post-1976-1977 periods. The SEIO index used in these computations is the time series constructed from the SST anomalies area-averaged over the domain 90°-122°E, 5°-45°S for the February-March season (see Fig. 1g).

There are a large number of observational and theoritical studies in the literature showing that the upper equatorial Pacific heat content is a key-precursor of ENSO during the boreal winter preceding the onset of the event (Wyrtki, 1985; Jin, 1997; Meinen and McPhaden, 2000; Hasegawa and Hanawa, 2003). On the other hand, McPhaden et al. (1998) put emphasis on the role of random westerly wind bursts on the

initiation of ENSO. These westerly anomalies occurring over the western equatorial Pacific can induce eastward propagating equatorial Kelvin waves and have been suggested as a possible trigger of the South America coastal warming. The westerly wind anomalies over the equatorial western Pacific and the anomalous equatorial Pacific upper ocean heat content are two excellent ENSO predictors that can predict across the boreal spring (Clarke and Van Gorder, 2001; Clarke and Van Gorder, 2003). It is therefore interesting to compare the predictive skills associated with our SEIO SST index and these other well-established ENSO precursors for both the pre- and post-1976-1977 periods. Following Clarke and Van Gorder (2003), we computed a February-March equatorial western Pacific zonal wind index (WPAC hereafter) as the time series of area-averaged zonal wind for the domain 130°-160°E, 5°S-5°N from the COADS dataset. Similarly, we defined a February-March upper ocean heat content index as the two-monthly mean 20°C thermocline depth (Z20 hereafter) area-averaged over the equatorial Pacific (130°E-80°W, 5°S-5°N) from the SODA product.

Focusing on the prediction of Niño3.4 SST evolution, we observe that the various ENSO precursors have different relationships with Niño3.4 SST before and after the 1976-77 regime shift (Fig. 2). This is especially true for both WPAC and SEIO indices, while the differences are only marginal for Z20. During the 1948-76 period Z20 is the best predictor, with values around 0.55 for the end of the year, whereas WPAC barely reaches values of around 0.35 for the same seasons. Apparently, El Niño events developed in the absence of significant westerly wind anomalies over the equatorial western Pacific prior to 1976. Finally, the SEIO SST index cannot be considered as a precursor of ENSO during the 1948-1976 period, a result consistent with Figure 1. Another interesting feature is the clear association between ENSO transitions and Z20

during the 1948-1976 period as the monthly correlations evolve from highly negative to highly positive from January to December of the El Niño year.

Turning now to the more recent period, all three indices emerge as good precursors of ENSO transition phases. SEIO is however the most effective, with correlation values exceeding those associated with Z20 and WPAC from September to December, and reaching a maximum of -0.76 in October (consistent with findings of Terray et al., 2004). The fact that both WPAC and SEIO indices are now significantly associated with ENSO transitions is also very intriguing. Thus, Figure 2 confirms the findings about the active role of Indian Ocean SSTs on ENSO evolution during recent decades. That is, from an observational viewpoint, our correlation analysis suggests that the SEIO index is a highly significant predictor in order to statistically predict the ENSO evolution during recent decades as the traditional Z20 or WPAC indices.

Figure 2 also suggests that the cold (warm) SEIO SST anomaly observed in February-March just before the onset of El Niño (La Niña) is not well correlated with the anomalous state of the Pacific Ocean during the preceding boreal winter since the correlations of February-March SEIO SSTs with January-February-March Niño3.4 SSTs are quite modest, particularly during recent decades. Other factors must be responsible for the emergence of anomalous SSTs off Australia during boreal winter after the 1976-77 regime shift.

4. Coupled air-sea interactions in the SEIO and the response of the climate system

In order to understand how the atmosphere and the ocean may interact to produce the SEIO SST anomaly, and leading to the observed correlations between SEIO and

Niño3.4 SST, we correlate the February-March SEIO SST index with 2-month average SST and SLP fields for both the pre- and post-1976-1977 periods (Fig. 3). The SLP dataset used in these computations is the ERSLP analysis. The correlations are computed with the negative of the February-March SEIO SST index so that the polarity is consistent with the correlation fields with Niño3.4 SST displayed in Figure 1. Gridpoint tests with a 90% confidence level have also been performed on all fields and are shown by shading in Figure 3. To facilitate the discussion, we consider the situation in which the positive correlations arise from a negative February-March SEIO SST anomaly. In this case, the regions of positive correlations in Figure 3 can be interpreted as positive SST or SLP anomalies associated with the negative February-March SEIO SST anomalies.

The regions of positive correlations over the southern Indian Ocean (near 40°S) in Figures 3ae indicate that the emergence of a negative SEIO SST anomaly to the west of Australia during February-March is accompanied by a positive SST anomaly to the southeast of Madagascar during the two periods. This anomalous SST pattern is reminiscent of the subtropical Indian Ocean dipole events studied by Behera and Yamagata (2001). We will refer to this as the south Indian Ocean SST dipole, with its positive phase when there is a negative SEIO SST anomaly. The associated SLP correlation patterns suggest that February-March cold SEIO SST anomalies are associated with a positive phase of the Southern Oscillation (Trenberth and Caron, 2000), and a strengthening and southwestward shift of the Mascarene High (approximate center at 35°S and 85°E) during the pre-1976-1977 period (Fig. 3c; see also Terray et al., 2003). On the other hand, the contribution from a La Niña state in the Pacific Ocean seems much smaller than that from the Mascarene High during the post-

1976-1977 regime shift period (Fig. 3g). During recent decades, the February-March cold SEIO SST anomalies are mainly linked to Mascarene High pulses and associated surface wind forcing off the west coast of Australia via enhanced latent heat flux, ocean mixing and Ekman transport (Behera and Yamagata, 2001; Terray et al., 2004). The hypothesis that ENSO evolution is more dependent on the Mascarene High pulses in the late boreal winter after the 1976-77 regime shift was then examined through a lag correlation analysis of February-March and April-May SLP fields with the Niño3.4 SST index during the following boreal winter (December-January). The lag correlation maps obtained from recent decades (Figs. 4cd) are in excellent agreement with the correlation patterns depicted in Figures 3gh, while no significant correlations are observed during February-March over the tropical and subtropical Indian Ocean for the pre-1976-77 regime shift period (Fig. 4a). Before the 1976-1977 regime shift, the main February-March SLP signal is found over the North Pacific associated with variability of the strength of the subtropical high in this region (Fig. 4a). It is thus speculated that this SLP pattern may be associated to a weakening of the trades in the central Pacific which may have significant impacts on the El Niño evolution (Fig. 4b). The close association between Mascarene High pulses in late boreal winter and ENSO evolution during recent decades was further tested through a correlation analysis between February-March meridional wind time series off the west coast of Australia (90°-115°E, 15°-40°S), computed from COADS dataset, and December-January Niño3.4 SST. The results confirm that boreal winter Niño3.4 SST is sensitive to the wind anomaly pattern off Australia during the previous boreal winter after the 1976-77 regime shift, but not before, since the correlation reverses its sign and becomes significant at the 99% confidence level after the 1976-1977 regime shift (-0.17 for 1948-1976, but 0.52 for

1977-1997). Interestingly, Figure 3g also demonstrates that the February-March Mascarene High pulses are associated with a modulation of the midlatitude westerlies in the southern Indian and Pacific Oceans during recent decades. It has been suggested that Mascarene High pulses are related to the Antarctic Circumpolar Wave (ACW, see Peterson and White, 1998; Fauchereau et al., 2003). As noted by White et al. (2004), the ACW may influence the magnitude and phase of El Niño in the eastern equatorial Pacific Ocean through an Indian Ocean pathway during recent decades. These connections need further investigations, but are outside of the scope of this study.

The SST and SLP correlation patterns observed during April-May, after the occurrence of a positive south Indian Ocean SST dipole event, are strikingly different in the pre- to post-1976-1977 regime shift periods (Fig. 3). During the first period, the SST correlation pattern in the southern Indian Ocean quickly fades away during boreal spring (Fig. 3b). Moreover, significant SLP correlations are restricted to the western Indian and eastern tropical Pacific Oceans (Fig. 3d). The Indian Ocean SLP correlation pattern suggests a delayed westward seasonal migration of the Mascarene High from boreal winter to boreal summer (Terray et al., 2003). On the other hand, if one interprets the region of negative correlations in Figure 3f as arising from a cold February-March SEIO SST anomaly, the April-May SST Indian Ocean correlation pattern indicates that the cold SEIO SST anomalies off the west coast of Australia persist and spread eastward between Australia and the Maritime Continent, reaching the vicinity of New Zealand in spring, during recent decades (Fig. 3f). As one would expect from quasi-geostrophic theory (Gill, 1982), an anomalous anticyclone is observed over or slightly to the west of the cold SEIO SST anomaly, suggesting a decrease in convection over the tropical eastern Indian Ocean in April-May, after the occurrence of a positive south Indian

Ocean SST dipole event during recent decades (Fig. 3h). Surprisingly, significant SST and SLP correlation patterns are also observed during spring in the mid and high latitudes of the South Pacific after 1977 (Figs. 3fh). These south Pacific SST anomalies are consistent with the development of the southern branch of the "horseshoe" ENSO pattern during recent decades (compare Figs. 1h and 3f). At the same time, the structure of the positive and negative SLP lagged correlations over the South Pacific (Fig. 3h) suggests the existence of a quasi-stationary Rossby wave train forced by anomalous equatorial convection that then propagates downstream in the midlatitude westerlies of the southern hemisphere (Sardeshmukh and Hoskins, 1987; Rasmusson and Mo, 1993; Trenberth et al., 1998). Moreover, the expanded trough observed in the South Pacific implies a weakening the subtropical SLP gradient around the South Pacific subtropical high and thus reduces the trade winds off the South America coast (see Fig. 5a), which then lead to the emergence of warm SST anomalies in the southeast subtropical Pacific during spring (Fig. 3f). van Loon and Shea (1987) and van Loon et al. (2003) emphasize the possible role of this expanded trough in the onset of El Niño events. Thus, the boreal late winter and spring evolution of SLP and SST correlation patterns suggests that the atmospheric anomalies (e.g. the Mascarene High pulses) are causing the SEIO SST anomalies, which in turn provide a strong positive feedback to the whole ocean-atmosphere system during spring in the post-1976-77 regime shift period. This point of view has been further substantiated by Terray et al. (2004) through composite analyses with respect to a February-March SEIO SST index for the post 1976-77 regime shift period.

To further illustrate the evolution of atmospheric patterns during the spring following the emergence of boreal winter SEIO SST anomalies after the 1976-1977

regime shift, we have computed regression coefficients between several fields (850 and 300 hPa winds, 500 hPa vertical velocity, 300 hPa geopotential height and precipitation) versus the February-March SEIO SST time series at various lags, a subset of which are given here (Fig. 5). These calculations make use of bi-monthly time series from the NCEP-NCAR reanalysis and gridded CMAP dataset. The sign of the regression coefficients has also been reversed, so that the polarity is consistent with the correlation plots in Figures 1, 3 and 4.

During boreal spring of cold SEIO SST years, the 850 hPa wind and 500 hPa vertical velocity regression patterns first confirm the existence of a weakening of the Inter Tropical Convergence Zone (ITCZ) in the subtropical Indian Ocean, with strong anomalous divergence (downward motion) and anticyclonic circulation over the eastern Indian Ocean colocated with the cold SSTs (Fig. 5a). Anomalous convergence (upward motion) and cyclonic circulation is also observed southeast of Madagascar. The atmospheric response to the SEIO SST forcing is also illustrated by the barotropic vertical structure of the pressure, height and wind anomalies, which have the same polarity throughout the troposphere southeast of Madagascar. The surface southeasterly wind anomalies associated with the anomalous anticyclone over the eastern Indian Ocean (Fig. 5a) represent an increase in wind speed relative to climatology between Java-Borneo and Australia, due to the reversal of the monsoon winds which is observed over this region during boreal spring. This implies further cooling of SST, northeastward of the anomalous subsidence center, via increased upper ocean mixing and evaporation (Fig. 3f). These cold SST anomalies further decrease the atmospheric convection, reinforcing the heat sink at higher levels (as suggested by the negative geopotential height anomalies over the eastern Indian Ocean and northwest Australia in

Figure 5b) which, in turn, maintains the anomalous SEIO anticyclone to the west (Fig. 3h). These processes represent a seasonally-positive feedback between the wind, evaporation and SST (Li et al., 2003; Wang et al., 2003) which allows the persistence of the SEIO SST anomalies after the occurrence of a south Indian Ocean dipole event. It may also explain the northward and eastward shift of the cold SST anomalies and associated anomalous anticyclone during the following months (Figs. 1h-k; see also Terray et al., 2004). In the subsequent boreal summer and fall, a positive wind-thermocline-SST feedback, off the west coast of Sumatra, may also contribute to the life cycle of the cold SST anomalies and associated anticyclone in the eastern Indian Ocean, as suggested by the SST TIOD pattern during October-November of the El Niño year seen in Figure 1k (Li et al., 2003; Terray et al., 2004). Furthermore, the strengthening of the monsoon winds over the eastern Indian Ocean, resulting from the anomalous SEIO anticyclone (Figs. 3h and 5a), may be a trigger of this another positive seasonal feedback operating off the west coast of Sumatra (Li et al., 2003, Terray et al. 2004).

The strength of the atmospheric signal associated with the cold SEIO SST anomaly is also manifest in the existence of westerly wind anomalies over the equatorial western Pacific (Fig. 5a). The large anomalous cyclonic circulation over the northwestern Pacific bears a strong resemblance with the Philippine Sea (El Niño) onset cyclone described in Wang (1995) as a key precursor of ENSO events after the 1976-77 regime shift. Thus, the 850 hPa wind regression map suggests that the anomalous SEIO anticyclone constructively interacts with the Philippine Sea (El Niño) onset cyclone to produce persistent and highly significant westerly wind anomalies over the western equatorial Pacific during cold SEIO SST years (Fig. 5a). Consistent with this hypothesis, we also observed anomalous convergence and positive rainfall anomalies

over the western Pacific, just west of the date line, while no significant SST anomalies are noted in these areas (Figs. 3f and 5ac). When SSTs are sufficiently high (e.g. above 25.5°C) as they are in the western Pacific warm pool, convection is strongly modulated by other factors, such as the atmospheric low-level convergence or upper-level divergence generated by remote forcing. These ideas are in harmony with findings of Lau et al. (1997) who stress the importance of large-scale circulation for convection to occur even though a high absolute SST is also a necessary condition (Graham and Barnett, 1987). Furthermore, Watanabe and Jin (2002) demonstrate with a linear baroclinic model that both Indian Ocean SST and the modulation of the ITCZ over the Indian Ocean are very important contributing factors for the development of the Philippine Sea anomalous cyclone/anticyclone through changes in the Walker circulation induced by convective cooling over the eastern Indian Ocean and Maritime Continent.

The cold SEIO SST anomalies and the anomalous anticyclone also seem to be associated with a northward shift of the Australian High (approximate center at 30°S and 130°E), and an earlier onset of the Australian winter monsoon in April-May, as seen in the strengthening of the regional meridional Hadley cell over the southwest Pacific with increased southward flow at 300 hPa and northward flow at 850 hPa (Figs. 5ab). This again favors the low-level convergence, but also an upper-level divergence over the west-central Pacific, and promotes the eastward propagation of equatorial westerly wind anomalies (Xu and Chan, 2001). Furthermore, this modulation of the meridional overturning over the southwest Pacific induces anomalous convergence at 300 hPa in the subtropics near the descending branch of the Hadley circulation (Fig. 5b). This upper-level anomalous convergence center, off the east coast of Australia,

seems then to act as a source of Rossby waves that force quasi-stationary upper-level circulation anomalies in the south Pacific extratropics, as depicted by the alternating high and low geopotential anomalies in the 300 hPa height regression map (Sardeshmukh and Hoskins, 1987; Rasmusson and Mo, 1993; Trenberth et al., 1998). The negative 300 hPa height anomalies to the east of New Zealand, resulting from this Rossby wave response, appear to induce a significant equatorward displacement of the upper level jet stream in the south Pacific (Fig. 5b). These changes in the location of the westerly jet stream may then impact the low-level circulation, as seen in Figures 3h, 4d and 5a, since the jet stream acts as a storm guide in the extratropical southern hemisphere (Trenberth, 1991; Trenberth et al., 1998; Bhaskaran and Mullan, 2003). This hypothesis is consistent with the equivalent barotropic structure observed in the mid-latitudes of the south Pacific, after positive south Indian Ocean dipole events, as depicted by the correlations of both SLP and 300 hPa height fields with the February-March SEIO SST index (Figs. 3h and 5b). In other words, there is a suggestion that the impact of the SEIO SST anomalies on the extratropical circulation in the South Pacific is indirect, and must be viewed through the modulations of the western Pacific regional Hadley cell.

Thus, the anomalous SEIO anticyclone may amplify the effect of random westerly wind bursts (McPhaden et al., 1998) or anomalous westerlies associated with the Philippine Sea onset cyclone (Fig. 5a; see Wang, 1995), and influence the development of El Niño after the 1976-1977 regime shift (Fig. 2). But, why did the cold SST SEIO anomalies and associated anomalous anticyclone fail to do so prior to 1976 (Fig. 2)?

5. Role of the decadal fluctuation in the SST background state

The SST is key in the two-way communication between the atmosphere and the ocean. Both the efficiency of the wind-evaporation-SST feedback and the intensity of convection increase with SST between about 26°C and 30°C, and thus depend critically on the SST background state (Graham and Barnett, 1987). That is, the wind-evaporation-SST feedback is muted by some nonlinear effects that come into play, if and only if, the underlying ocean is sufficiently warm, say above 26°C, because the nonlinear relationship between convection and SST becomes pronounced above this treshold (Gill, 1982). Furthermore, the spatial extension of the region concerned by this positive feedback is also controlled by the climatological SST.

A key aspect of the decadal fluctuation in the background state is the abrupt warming of the Indian Ocean around 1976-1977 (Nitta and Yamada, 1989; Terray, 1994; Aoki et al., 2003). Thus, the 1976-77 climate shift, whether part of decadal variability or global warming trend influences the climatic background of SST in the Indian Ocean. This is well illustrated in the differences between the April-May mean SST over the Indian and Pacific Oceans before and after the 1976-1977 regime shift (Fig. 6a). The statistical significance of these epoch SST differences (Fig. 6b) has been assessed using a permutation procedure with 9999 shuffles described in Terray et al. (2003). This method determines the areas in the SST differences map that depart significantly from the background variability in the available data. The 1976-1977 climate shift leads to substantial warming in the whole Indian Ocean, but is particularly significant and prominent in the southern Indian Ocean at subtropical latitudes, and off the west coast of Australia, where the rise in SST exceeds 0.5°C during spring.

Although the magnitudes of the SST differences in the Indian Ocean are smaller than those observed in the North Pacific (Fig. 6a), they are in fact much more statistically significant due to a weaker background interannual variability (Fig. 6b).

This critical aspect of the 1976-77 climate regime shift has been overlooked in the past. Thus, the Indian Ocean warming observed after 1976-1977 seems to be more influential in strengthening the seasonally positive wind-evaporation-SST feedback over the SEIO during boreal spring, as warm waters above 26°C spread southward after 1977. This SST change is also consistent with an increased efficiency of the wind-evaporation-SST feedback during recent decades, as depicted by Figures 3 and 5. We speculate that this spatial extension of the Indian Ocean warm pool may explain the stronger links between southern Indian Ocean variability in boreal winter and the ENSO evolution observed after the 1976-1977 regime shift (Figs. 1, 2 and 4; see also Terray et al., 2004).

Consistent with this hypothesis, the April-May standard deviations of SST and SLP fields in the eastern Indian Ocean have both increased after the 1976-1977 regime shift (not shown). The stronger coupling of these two fields in the eastern Indian Ocean during boreal spring after the 1976-77 regime shift can also be illustrated through the SVD analysis of the covariance matrix of the SLP and SST fields (Bretherton et al., 1992). Figures 7 and 8 show the leading modes derived from the SVD analysis of the April-May SST and SLP fields over the tropical Indian Ocean (30°-120°E, 34°S-30°N) for both the 1948-1976 and 1977-2001 periods. In the terminology of Bretherthon et al. (1992), the fields presented from the SVD analyses, and shown in Figures 7 and 8, are heterogeneous (covariance) patterns for SLP and homogeneous patterns for SST. Table

1 presents summary statistics for the two SVD analyses, including the Squared Covariance Fraction (SCF), the Normalized root-mean-square Covariance (NC) for the leading modes in the various SVD expansions and the correlation coefficient (r) between the expansion coefficient time series (or scores) of the left and right fields. As discussed by Zhang et al. (1998), the NC and r coefficients are particularly useful in comparing the strength of the relationship between the right and left fields in modes obtained from different SVD analyses. Thus, these statistics are useful tools to investigate the strength of the positive wind-evaporation-SST feedback over the SEIO during boreal spring before and after the 1976-1977 regime shift.

The SCF/NC/r for the first mode derived from the 1977-97 time interval are 55/21/0.85 compared to 57/15/0.62 for its 1948-76 counterpart. Moreover, the first SVD mode accounts for 42% of the SLP variance during the 1977-97, but for only 36% before the 1976-1977 regime shift. Thus, the summary statistics, shown in Table 1, suggest that the April-May Indian Ocean SST and SLP fields are more strongly coupled after the 1976-77 regime shift, even though the SCF coefficient is slightly higher before the 1976-77 regime shift.

During both periods, the dominant features in the SLP and SST spatial patterns of the leading SVD modes are located in the southern hemisphere (Figs. 7 and 8). Yet despite this similarity, the spatial representations of these leading covarying modes are also strikingly different between the two periods. The leading singular vectors for the SVD expansion computed on recent decades (Figs. 8ab) resemble the Indian Ocean portion of the April-May SLP and SST regression patterns computed upon the February-March SEIO SST time series (Figs. 3fh) whereas this similarity is not evident

for the leading singular vectors and regression maps computed from the 1948-1976 period, particularly for the SLP field. The correlation coefficients between the SVD expansion coefficient time series and the February-March SEIO SST time series (Table 2) lend credence to this feature with correlations as high as –0.62 and –0.68 for the SLP and SST scores during the 1977-1997 period, whereas the corresponding coefficients computed from the 1948-1976 period are only –0.35 and –0.5, respectively. It is also worth noting that the correlation coefficient between the SLP scores and the February-March SEIO SST time series is highly significant after the 1976-1977 regime shift, according to the phase-scrambling bootstrap test, while its 1948-1976 counterpart is not significant at the 95% confidence level (Table 2). Thus, it appears that the southern Indian Ocean SLP and SST fields are more strongly coupled during boreal spring after the 1976-1977 shift and this seems to be related to SEIO SST variability during late boreal winter associated with south Indian Ocean SST dipole events and to the warmer SEIO climatological SSTs observed during recent decades. This is further demonstrated if we look at the lagged correlations between February-March SEIO SSTs and the subsequent evolution of the SLP and SST patterns prior to 1976 (Fig. 3). The atmospheric signal associated with the SEIO SST anomalies is weaker and quite different in character compared to those derived from the recent period. Moreover, cold SEIO SST years are not associated with the growth of an El Niño event before 1976 (Figs. 1 and 2).

6. Discussion and Conclusions

The present paper calls attention to one critical aspect of the decadal variation of ENSO properties which has been overlooked in previous studies. The 1976-1977 regime

shift was accompanied by a remarkable and significant change in the lead-lag relationships between Indian Ocean SSTs and El Niño evolution. This change is so prominent, that, from an observational view point, southern Indian Ocean SSTs during late boreal winter are a highly significant precursor of the ENSO evolution after the 1976-77 regime shift. This relationship was also documented in Terray et al. (2004) with different methods and observational datasets.

The possible physical mechanisms, underlying this surprising and highly significant statistical relationship, observed only during recent decades, are discussed through a comprehensive analysis of a wide variety of new observational and reanalysis datasets. During recent decades, the SEIO SST anomalies are mainly generated by Mascarene High pulses occurring in late boreal winter (Behera and Yamagata, 2001). The results suggest that these SEIO SST anomalies observed during boreal winter play a fundamental role in the ENSO transitions after the 1976-77 regime shift, by triggering coupled air-sea processes in the tropical eastern Indian Ocean during the following boreal spring, summer and fall. It is hypothesized that the interdecadal change in the background SST state that occurred in the late 1970s over the Indian Ocean significantly influences the nature of the air-sea interactions over the SEIO during boreal spring. More precisely, we argue that the recent Indian Ocean warming may have considerably amplified the seasonally-positive wind-evaporation-SST feedback over the SEIO (Li et al., 2003; Wang et al., 2003; Terray et al., 2004), due to an increase in SST values above which the nonlinear relationship between convection and SST becomes pronounced (e.g. 26°C; Gill, 1982). This hypothesis is based on the results of SVD analyses conducted on Indian Ocean SST and SLP fields, separately, for the 1948-1976 and 1977-1997 periods. In the leading covarying mode during boreal spring, SLP and

SST patterns differ considerably from the first period to the last. Moreover, the results from recent decades are consistent with a strengthening of the coupling between the SST and SLP fields in the South Indian Ocean and, particularly, over the SEIO.

The above scenario of a more efficient wind-evaporation-SST feedback in the eastern Indian Ocean after the 1976-77 regime shift offers some clues as to how boreal winter SEIO SST anomalies may have helped to trigger El Niño events or ENSO transitions in recent decades (Yu et al., 2003). This favours the persistence of SST anomalies and the associated atmospheric center in the eastern Indian Ocean, which then acts as a persistent remote forcing on the whole Pacific system by promoting wind anomalies over the western equatorial Pacific and modulating the regional Hadley cell in the southwest Pacific during boreal spring and early summer. The fluctuations in the intensity of this regional Hadley cell then excite Rossby waves in the southern extratropics, and are the medium through which the SEIO SST signal is propagated in the mid latitudes of the South Pacific. The resultant quasi-stationary circulation anomalies observed in the south Pacific seem, in turn, to be responsible for the development of the southern branch of the ENSO “horseshoe” pattern after the 1976-1977 climate shift. These results shed some light on the possible influence of global warming or decadal fluctuations on ENSO development and evolution through changes in teleconnection patterns between the Indian and Pacific Oceans.

To some extent, such a scenario could also explain why ENSO evolution is different before and after the 1976-1977 regime shift (An and Wang, 2000; Wang and An, 2001), with both the persistent variability of zonal wind anomalies over the equatorial western Pacific and the modulation of the Hadley cell over the southwest

Pacific induced by SEIO SST anomalies during recent decades. Our observational results demonstrate at least that the Indian Ocean cannot be considered a "slave" to ENSO after the 1976-1977 regime shift. As shown here, the Indian Ocean has its own modes of coupled variability and is significantly related to ENSO transitions after the 1976-1977 climate shift. Further quantitative exploration of ocean-atmosphere feedback processes existing in the Indian Ocean, and those which may be more active after the 1976-1977 regime shift, will evidently contribute to our understanding of why El Niño evolution has dramatically changed during recent decades. However, the exact role of SEIO SST anomalies in ENSO evolution cannot be elucidated without a more comprehensive investigation involving a quantitative evaluation of the fluxes at the air-sea interface in the SEIO before and after the 1976-1977 regime shift.

While we have stressed the importance of Mascarene High pulses during boreal winter in the generation of SEIO SST anomalies during recent decades, we did not address the important question of what actually causes these pulses. Clearly, the Mascarene High pulses are interrelated to various degrees with modes of variability in the southern hemisphere (Simmonds, 2003; Fauchereau et al., 2003; White et al., 2004) and these connections merit further study.

A thorough understanding of the interaction between the PDO and our coupled interannual mode is also important. The southern parts of the eastern Indian and western Pacific Oceans have been noted to exhibit large SST and SLP signals associated with the PDO (Deser et al., 2004). It is thus possible that the teleconnection patterns observed before and after 1976 when the PDO reportedly changed polarities are associated with different phases of the PDO. The recent decades include a tendency for

the PDO to be in a positive state (Mantua et al., 1997). It is unknown whether these decadal-scale background conditions influence the response of the tropical atmospheric circulation to SEIO SST anomalies, hence representing an important framework for the results found here. This raises the question of what the driving mechanisms of the warming trend and decadal signal in the Indian Ocean are, and how this decadal signal may interact with the interannual variability over the Indian and Pacific Oceans at decadal to secular time scales.

Another important issue is the possible relationship between the coupled interannual mode described here and the Madden-Julian Oscillation (MJO) which is the primary mode of intraseasonal (30-60 days) variations of the tropical troposphere (Madden and Julian, 1994). This question warrants further investigation since the MJO involves pronounced fluctuations in convection and large scale circulation during boreal winter over the eastern Indian and western Pacific Oceans as does our interannual coupled mode (Madden and Julian, 1994; Jones et al., 1998). Furthermore, the MJO manifests itself as a slow eastward propagation of atmospheric disturbances from the eastern Indian Ocean to the western Pacific Ocean and has been suggested to play a role in triggering ENSO events through the westerly wind bursts and associated Kelvin wave forcing, even though the interannual changes in overall MJO activity are not related to the ENSO cycle (Kessler et al., 1995; Hendon et al., 1999). Some studies have also suggested that this MJO-ENSO relationship is significant only for the recent period and that such evidence can not be found for time periods before the 1976-1977 climate shift (Zhang and Gottschalck, 2002). Most of these features are also significant characteristics of the interannual mode (Terray et al., 2004). However, some distinctive features may also be observed since the MJO is an equatorially trapped phenomenon

and the air-sea convective intraseasonal interaction involved in an eastward-moving MJO is fundamentally different from the wind-evaporation-SST feedback which seems to be the key mechanism in sustaining the interannual mode (Jones et al., 1998). In order to examine how the year-to-year variations in the intensity of the MJO activity relate to south Indian Ocean SST dipole events, we have correlated our February-March SEIO SST time series with an index of MJO activity for late austral summer of each year. This MJO index is the January-March mean of the sum of the squares of the two leading principal components derived from an empirical orthogonal function analysis of the combined fields of daily near-equatorially averaged 850-hPa zonal wind, 200-hPa zonal wind, and satellite-observed outgoing longwave radiation data (Wheeler and Hendon, 2004). We found no significant relationship between this MJO index and our SEIO SST time series, the correlation between the two being only –0.01 during the 1977-2001 period. The use of a SLP index monitoring the interannual variations of the Mascarene High during February-March does not change this result (correlation of –0.08). Furthermore, this MJO index is not a precursor of the ENSO evolution (correlation with October-November-December Niño3.4 SSTs of 0.03). Thus, the above preliminary analysis suggests that if MJO activity plays a role in maintaining the interannual coupled mode described here, the relationship between the two phenomena is strongly nonlinear. Further improved observational and theoretical studies are needed to resolve this issue.

It will also be of interest to determine whether current coupled models are capable of simulating the coupled interactions described in this paper. If so, the use of global coupled numerical ocean-atmosphere experiments with idealized conditions (e.g. a prescribed SEIO SST anomaly in February-March) may also be helpful in reaching

more definite conclusions about the role of SEIO SST anomalies in the coupled climate system during recent decades. Our current research is exploring this possibility. Finally, the findings reported here have important implications for ENSO predictability during recent decades.

Acknowledgements: The comments of the anonymous reviewers and the editor, T.G. Jensen, led to improvements in the manuscript. This work was supported by the French Programme National d'Etude Du Climat (PNEDC). The NCAR/NCEP reanalysis, COADS, ERSST, ERSLP and CMAP datasets were provided through the NOAA Climate Center (http://www.cdc.noaa.gov). SODA analysis data is from the IRI data library server (http://iridl.columbia.edu). The authors would like to thank T.M. Smith and R.W. Reynolds for providing their recent SST and SLP reconstruction datasets before publication. Computations were performed at the French Institute for Development and Resources in Scientific Computing (IDRIS). Graphics prepared using the SAXO package of Sébastien Masson. We thank A.S. Fischer and L. Terray for comments and careful re-reading of an earlier draft of this manuscript.

References

Alexander, M.A., et al., 2002: The Atmospheric Bridge : the Influence of ENSO Teleconnections on Air-Sea Interaction over the Global Oceans. *J. Climate*, **15***,* 2205-2231.

Allan, R.J., J.A. Lindesay and C.J.C. Reason, 1995: Multidecadal variability in the climate system over the Indian Ocean region during Austral summer. *J. Climate*, **8***,* 1853-1873.

Allan, R.J., and coauthors, 2001: Is there an Indian Ocean dipole, and is it independent of the El Nino-Southern Oscillation? *CLIVAR Exch.*, **6** (3),18-22.

An, S.-I., and B. Wang, 2000: Interdecadal change of the structure of the ENSO mode and its impact on the ENSO frequency. *J. Climate*, **13***,* 2044-2055.

Aoki, S., M. Yoritaka, and A. Masuyama, 2003: Multidecadal warming of subsurface temperature in the Indian sector of the southern ocean. *J. Geophys. Res.*, **108***,* 8081-8088.

Babu, C.B., and P.V. Joseph, 2002: Post-monsoon sea surface temperature and convection anomalies over Indian and Pacific Oceans. *Int. J. Climatol.*, **22**, 559-567.

Behera, S.K., and T. Yamagata, 2001: Subtropical SST dipole events in the southern Indian Ocean. *Geophys. Res. Lett.,* **28***,* 327-330.

Bhaskaran, B., and A.B. Mullan, 2003: El Niño-related variations in the southern Pacific atmospheric circulation: model versus observations. *Clim. Dyn.*, **20***,* 229-239.

Bretherton, C., Smith, C. & Wallace, J., 1992: An intercomparison of methods for finding coupled patterns in climate data. *J. Climate*, **5**, 541-560.

Carton, J.A., G. Chepurin, X. Cao, and B. Giese, 2000: A Simple Ocean Data Assimilation Analysis of the Global Upper Ocean 1950-95. Part 1: Methodology. *J. Phys. Oceanogr.*, **30***,* 294-309.

Clarke, A.J., and S. Van Gorder, 2001: ENSO prediction using an ENSO trigger and a proxy for western equatorial warm pool movement. *Geophys. Res. Lett.,* **28***,* 579-582.

Clarke, A.J., and S. Van Gorder, 2003: Improving El Niño Prediction using a Space-Time Integration of Indo-Pacific Winds and Equatorial Pacific Upper Ocean Heat Content. *Geophys. Res. Lett.,* **30***,* 52.1-52.4.

Davison, A.C., and D.V. Hinkley, 1997: Bootstrap methods and their application. 582 pp. Cambridge University Press, Cambridge, UK.

Deser, C., A.S. Philips, and J.W. Hurell, 2004: Pacific interdecadal climate variability: Linkages between the tropics and North Pacific during boreal winter since 1900. *J. Climate*, **17**, 3109-3124.

Ebisuzaki, W., 1997: A method to estimate the statistical significance of a correlation when the data are serially correlated. *J. Climate*, **10***,* 2147-2153.

Fauchereau, N., S. Trzaska, Y. Richard, P. Roucou and P. Camberlin, 2003: Sea-Surface Temperature co-variability in the southern Atlantic and Indian oceans and its connections with the atmospheric circulation in the Southern Hemisphere. *Int. J. Climatol.*, **23**, 663-677.

Garreaud, R.D., and D.S. Battisti, 1999: Interannual and interdecadal variability of the tropospheric circulation in the Southern Hemisphere. *J. Climate*, **12**, 2113-2123.

Gill, A.E., 1982: *Atmosphere-Ocean Dynamics.* 662 pp, Academic Press, New York.

Graham, N.E., and T.P. Barnett, 1987: Sea surface temperature, surface wind divergence and convection over tropical Oceans. *Science*, **238***,* 657-659.

Graham, N.E., 1994: Decadal scale variability in the tropical and North Pacific during the 1970s and 1980s: observations and model results. *Climate Dyn.,* **10***,* 135-162.

Guilderson, T.P., and D.P. Schrag, 1998: Abrupt shift in subsurface temperatures in the Tropical Pacific associated with changes in El Niño. *Science*, **281***,* 240-243.

Hasegawa, T., and K. Hanawa, 2003: Heat content Variability related to ENSO events in the Pacific. *J. Phys. Oceanogr.*, **33**, 407-421.

Hendon, H.H., C. Zhang, and J.D. Glick, 1999: Interannual variation of the Madden-Julian oscillation during austral summer. *J. Climate*, **12***,* 2538-2550.

Jin, F.F., 1997: An equatorial ocean recharge paradigm for ENSO. Part I: Conceptual model. *J. Atmos. Sci.*, **54**, 811-829.

Jones, C., D.E. Waliser, and C. Gautier, 1998: The influence of the Madden-Julian Oscillation on ocean surface heat fluxes and sea surface temperature. *J. Climate*, **11***,* 1057-1072.

Kachi, M., and T. Nitta, 1997: Decadal variations of the global atmosphere-ocean system. *J. Meteor. Soc. Japan.,* **75***,* 657-675.

Kalnay et al., 1996: The NCEP/NCAR 40-Year Reanalysis Project. *Bull. Amer. Meteor. Soc.*, **77***,* 437-471.

Kessler, W.S., M.J. McPhaden, and K.M. Weickmann, 1995: Forcing of intraseasonal Kelvin waves in the equatorial Pacific Ocean. *J. Geophys. Res.*, **100***,* 10 613-10 631.

Kinter, J.L., K. Miyakoda, and S. Yang, 2002: Recent change in the connection from the Asian Monsoon to ENSO. *J. Climate*, **15***,* 1203-1215.

Klein, S.A., B.J. Soden, and N.-C. Lau, 1999: Remote sea Surface Temperature Variations during ENSO: Evidence for a Tropical Atmospheric Bridge. *J. Climate*, **12***,* 917-932.

Kumar, K.K., B. Rajagopalan, and M.A. Cane, 1999: On the weakening relationship between the Indian monsoon and ENSO. *Science*, **284***,* 2156-2159.

Lau, K.M, H.T. Wu, and S. Bony, 1997: The role of large scale atmospheric circulation in the relationship between tropical convection and sea surface temperature. *J. Climate*, **10***,* 381-392.

Li, T., B. Wang, C.P. Chang, and Y.S. Zhang, 2003: A theory for the Indian Ocean dipole-zonal mode. *J. Atmos. Sci.,* **60***,* 2119-2135.

Madden, R.A., and P.R. Julian, 1994: Observations of the 40-50-day tropical oscillation: A review. *Mon. Wea. Rev.*, **112**, 814-837.

Mantua, N., S.J. Hare, Y. Zhang, J;M. Wallace and R.C. Francis, 1997: A Pacific interdecadal oscillation with impacts on salmon production. *Bull. Amer. Meteor. Soc.,* **78***,* 1069-1079.

McPhaden, M.J., and coauthors, 1998: The tropical ocean global atmosphere observing system: A decade of progress. *J. Geophys. Res.*, **103***,* 14169-14240.

Meinen, C.S., and M.J. McPhaden, 2000: Observations of warm water volume changes in the equatorial Pacific and their relationship to El Niño and La Niña. *J. Climate*. **13**, 3551-3559.

Nitta, T., and S. Yamada, 1989: Recent warming of tropical sea surface temperature and its relationship to the Northern Hemisphere. *J. Meteor. Soc. Japan.,* **67***,* 375-383.

Nitta, T., and M. Kachi, 1994: Interdecadal variations of precipitation over the tropical Pacific and Indian Oceans. *J. Meteor. Soc. Japan.,* **72***,* 823-831.

Noreen, E.W., 1989: Computer-intensive methods for testing hypotheses: an introduction. John Wiley & Sons, New York.

Peterson, R., and W.B. White, 1998: Slow oceanic teleconnections linking tropical ENSO and the Antarctic circumpolar wave. *J. Geophys. Res.*, **103**, 24,573-24,583.

Rao, K.G., and B.N. Goswami, 1988: Interannual variations of sea surface temperature over the Arabian Sea and the Indian monsoon: a new perspective. *Mon. Weath. Rev.*, **116**, 558-568.

Rasmusson, E.M., and K. Mo, 1993: Linkages between 200-mb tropical and extratropical circulation anomalies during the 1986-1989 ENSO cycle. *J. Climate*, **6***,* 595-616.

Rayner, N.A., Parker, D.E., Horton, E.B., Folland, C.K., Alexander, L.V., Rowell, D.P., Kent, E.C., and A. Kaplan, 2003: Global analyses of sea surface temperature, sea ice, and night marine air temperature since the late nineteenth century. *J. Geophys. Res.*, **108** (D14), 4407, doi:10.1029/2002JD002670.

Saji, N.H., B.N. Goswami, P.N. Vinayachandran, and T.A. Yamagata, 1999: Dipole Mode in the Tropical Indian Ocean. *Nature*, **401***,* 360-363.

Sardeshmukh, P.D., and B.J. Hoskins, 1987: The generation of global rotational flow by steady idealized tropical divergence. *J. Atmos. Sci.*, **45***,* 1228-1251.

Sewell, R., D., and W.A. Landman, 2001: Indo-Pacific relationships in terms of sea-surface temperature variations. *Int. J. Climatol.*, **21**, 1515-1528.

Simmonds, I., 2003: Modes of atmospheric variability over the Southern Ocean. . *J. Geophys. Res.*, **108**(C4), 8078, doi:10.1029/2000JC000542.

Smith, T.M., and R.W. Reynolds, 2002: Extended Reconstruction of Oceanic Sea–Level Pressure Based on COADS and Station Data (1854-1997). *J. Oceanic. Atmos. Tech*., submitted.

Smith, T.M., and R.W. Reynolds, 2003: Extended Reconstruction of Global Sea Surface Temperatures Based on COADS Data (1854-1997). *J. Climate.* **16**, 1495-1510.

Smith, T.M., and R.W. Reynolds, 2004: Improved Extended Reconstruction of SST (1854-1997). *J. Climate,* **17***,* 2466-2477.

Terray, P., 1994: An evaluation of climatological data in the Indian ocean area. *J. Meteor. Soc. Japan*., **72***,* 359-386.

Terray, P., 1995: Space/Time structure of monsoons interannual variability. *J. Climate*, **8**, 2595-2619.

Terray, P., P. Delecluse, S. Labattu, and L. Terray, 2003: Sea Surface Temperature Associations with the Late Indian Summer Monsoon. *Clim. Dyn.*, **21***,* 593-618.

Terray, P., S. Dominiak, and P. Delecluse, 2004: Role of the southern Indian Ocean in the transitions of the monsoon-ENSO system during recent decades. *Clim. Dyn*., in press.

Trenberth, K.E., 1991: Storm tracks in the Southern Hemisphere. *J. Atmos. Sci.*, **48***,* 2159-2178.

Trenberth, K.E., and J.W. Hurell, 1994: Decadal atmosphere-ocean variations in the Pacific. *Climate Dyn.,* **9***,* 303-319.

Trenberth, K.E., et al., 1998: Progress during TOGA in understanding and modeling global teleconnections associated with tropical sea surface temperatures. *J. Geophys. Res.*, **103***,* 14291-14324.

Trenberth, K.E., and J.M. Caron, 2000: The Southern Oscillation revisited: Sea Level Pressures, Surface Temperatures, and Precipitation. *J. Climate*, **13***,* 4358-4365.

Trenberth, K.E., J.M. Caron, D.P. Stepaniak, and S. Worley, 2002: The evolution of ENSO and global atmospheric surface temperatures. *J. Geophys. Res.*, **107***,* D8, 10.1029/2000JD000298.

Van Loon, H., and D.J. Shea, 1987: The Southern Oscillation. Part VI : Anomalies of sea level pressure on the Southern Hemisphere and of Pacific sea surface temperature during the development of a warm event, *Mon. Wea. Rev.*, **115**, 370-379, 1987.

Van Loon, H., G.A. Meehl and R. Milliff, 2003: The Southern Oscillation in the early 1990s. *Geophys. Res. Lett.*, **30**, 311-314.

Wallace, J., et al., 1998: On the structure and evolution of ENSO-related climate variability in the tropical Pacific: Lessons. *J. Geophys. Res.* **103***,* 14241-14259.

Wang, B., 1995: Interdecadal changes in El Nino onset in the last four decades. *J. Climate*, **8***,* 267-285.

Wang, B., and S.-I. An, 2001: Why the Properties of El Niño Changed during the Late 1970s. *Geophys. Res. Lett.,* **28***,* 3709-3712.

Wang, B., Wu, R., and K.-M. Lau, 2001: Interannual Variability of the Asian Summer Monsoon: Contrasts between the Indian and the Western North Pacific–East Asian Monsoons. *J. Climate*, **14**, 4073-4090.

Wang, B., R. Wu, and T. Li, 2003: Atmosphere-Warm Ocean Interaction and its Impacts on Asian-Australian Monsoon Variation. *J. Climate*, **16***,* 1195-1211.

Watanabe, M., and F.-F. Jin, 2002: Role of Indian Ocean warming in the development of Philippine Sea anticyclone during ENSO. *Geophys. Res. Lett.,* **29***,* doi: 10.1029/2001GL014318.

Webster, P.J., et al., 1998: Monsoons: Processes, Predictability and the Prospects for Prediction. *J. Geophys. Res.,* **103***,* 14451-14510.

Wheeler, M.C., and H.H. Hendon, 2004: Interannual variation of the Madden-Julian oscillation during austral summer. *Mon. Wea. Rev.*, **132***,* 1917-1932.

White, W.B., and J. Annis, 2004: Influence of the Antarctic Circumpolar Wave on El Niño and its multidecadal changes from 1950-2001. *J. Geophys. Res.*, **109**(C0), 6019, doi:10.1029/2002JC001666.

Woodruff, S.D., H.F. Diaz, J.D. Elms, and S.J. Worley, 1998: COADS Release 2 data and metadata enhancements for improvements of marine surface flux fields. *Phys. Chem. Earth,* **23***,* 517-527.

Wu, R., and B.P. Kirtman, 2004: Impacts of the Indian Ocean on the Indian Summer Monsoon-ENSO relationship. *J. Climate,* **17***,* 3037-3054.

Wyrtki, K., 1985: Water displacements in the Pacific and the genesis of El Niño cycles. *J. Geophys. Res.*, **90**, 7129-7132.

Xie, P., & P.A. Arkin, 1997: Global Precipitation: a 17-year Monthly Analysis Based on Gauge Observations, Satellite Estimates, and Numerical Outputs. *Bull. Am. Meteo. Soc.*, **78***,* 2539-2558.

Xu, J., and J.C.L. Chan, 2001: The Role of the Asian-Australian Monsoon System in the Onset Time of El Nino Events. *J. Climate,* **14***,* 418-433.

Yamagata, T., and coauthors, 2002: The Indian Ocean dipole: A physical entity. *Clivar Exch.*, **7** (2), 15-18.

Yu, J.-Y., S.-P. Weng, and J.D. Farrara, 2003: Ocean Roles in the TBO Transitions of the Indian-Australian Monsoon System. *J. Climate,* **16***,* 3072-3080.

Zhang, C., and J. Gottschalck, 2002: SST anomalies of ENSO and the Madden-Julian Oscillation in the equatorial Pacific. *J. Climate*, **15**, 2429-2445.

Zhang, Y., Wallace, J.M. and D.S. Battisti, 1997: ENSO-like interdecadal variability : 1900-1993. *J. Climate*, **10**, 1003-1020.

Zhang, Y., J.R. Norris, and J.M. Wallace, 1998: Seasonality of large scale atmosphere-ocean interaction over the North Pacific. *J. Climate*, **11**, 2473-2481.

Figure captions

Figure 1: Time sequence of correlations with December-January Niño3.4 (5°S-5°N/190°E-240°E) SST time series of Indo-Pacific SSTs at –5 to 0 bi-monthly seasons for 1948-1976 (panels a, b, c, d, e, f) and 1977-2001 (panels g, h, i, j, k, l) periods. The maps only show correlations that are above the 90% confidence level estimated with a phase-scrambling bootstrap test with 999 samples.

Figure 2: Lead-lag correlations of monthly Niño3.4 SST index with February-March South East Indian Ocean SST (SEIO: 90°E-122°E/5°S-45°S, in black-filled symbols), Western PACific zonal wind (WPAC: 130°E-160°E/5°N-5°S, in grey-filled symbols) and equatorial Pacific mean 20°C thermocline depth (Z20: 130°E-280°E/5°N-5°S, open symbols) time series for 1948-1946 (circles) and 1977-2001 (squares) periods –except for WPAC, available until 1997-. The sign of some correlations has been reversed (noted "-opp." in the legend) in order to facilitate comparisons between the various ENSO predictors and periods.

Figure 3: Correlation analysis of February-March SEIO SST time series with February-March (labelled "FM") and April-May (labelled "AM") SST (left) and SLP (right) fields for 1948-1976 (panels a, b, c, d) and 1977-2001 (or 1977-1997 for SLP, panels e, f, g, h) periods. The correlations are computed with the negative of the SEIO SST time series so the polarity is consistent with the Niño3.4 correlation plots seen in Figure 1. Correlations significant at the 90% confidence level following a phase-scrambling bootstrap procedure with 999 samples are shaded.

Figure 4: Correlation analysis of December-January Niño3.4 SST time series with February-March and April-May (prior to December-January) Indo-Pacific SLP fields

for 1948-1976 (panels a and b) and 1977-1997 (panels c and d) periods, respectively. Correlations significant at the 90% confidence level following a phase-scrambling bootstrap procedure with 999 samples are shaded.

Figure 5: Distribution of the regression coefficients of April-May 850 (a) and 300 (b) hPa wind vectors (arrows, see scales below the panels), 500 hPa vertical velocity (a: color shading, upward is negative), 300 hPa geopotential height (b: color shading) and precipitation (c: color shading) versus the February-March SST index for the SEIO region. The regression coefficients are computed from the 1979-2001 period for precipitation and 1977-2001 for other variables. The convention for the colour shading is indicated at the bottom of the panels. Note that the regression coefficients are computed with the negative of the SEIO SST time series. The maps only show regression coefficients that are above the 90% confidence level following a phase-scrambling procedure with 999 samples.

Figure 6: April-May SST differences between the 1977-2001 and 1948-1976 periods (a). Significance levels (or critical probabilities) associated with the SST difference values in (a) are shown in (b). These critical probabilities have been assessed using a permutation procedure with 9999 shuffles (Terray et al., 2003). Only, the 90 (clear gray), 99 (dark gray), 99.9 (black) % confidence levels are drawn in (b).

Figure 7: The leading boreal spring mode of coupled year to year variability in (a) SST and (b) SLP over the Indian Ocean (30°-120°E, 34°S-30°N) as inferred from SVD analysis of seasonal-mean (April-May) fields during the 1948-1976 period. The contours values were obtained by regressing the SLP and SST fields upon the normalized expansion coefficient time series of SST. The SST and SLP fields are,

respectively, homogenous and heterogeneous covariance patterns following the terminology of Bretherton et al. (1992). Summary statistics for this mode are given in Table 1.

Figure 8: Same as Figure 7, but for the leading boreal spring mode of coupled year to year variability in (a) SST and (b) SLP of seasonal-mean (April-May) fields during the 1977-1997 period. Summary statistics for this mode are given in Table 1.

Table Captions

Table 1: Summary statistics for the leading mode of the SVD analyses for the April-May Indian Ocean SST field paired with the Indian Ocean SLP field during the 1948-1976 and 1977-1997 periods. Here SCF is squared covariance fraction, NC is normalized root-mean-square and *r* is correlation of expansion coefficient time series or scores; SLPvar and SSTvar are, respectively, SLP and SST variances accounted for by the leading mode of each SVD analysis.

Table 2: Correlation coefficients of February-March SEIO SST time series with the expansion coefficient time series (scores) of the left (SST) and right (SLP) fields associated with the leading SVD mode during the 1948-1976 and 1977-1997 periods, respectively. Correlations significant at the 95, 99% levels are marked with one or two stars, respectively. The statistical significance of the correlation coefficients has been assessed with a phase-scrambling bootstrap test with 999 sampled.

Tables

Table 1

	SCF(%)	NC(%)	*r*	SLPvar(%)	SSTvar(%)
1948-1976	57.6	14.9	0.62	36.1	15.7
1977-1997	54.8	21.3	0.85	42	15

Table 2

	SEIO SST (2-3) with SST scores of the leading SVD mode	SEIO SST (2-3) with SLP scores of the leading SVD mode
1948-1976	-0.50**	-0.35
1977-1997	-0.68**	-0.61**

Figure 1

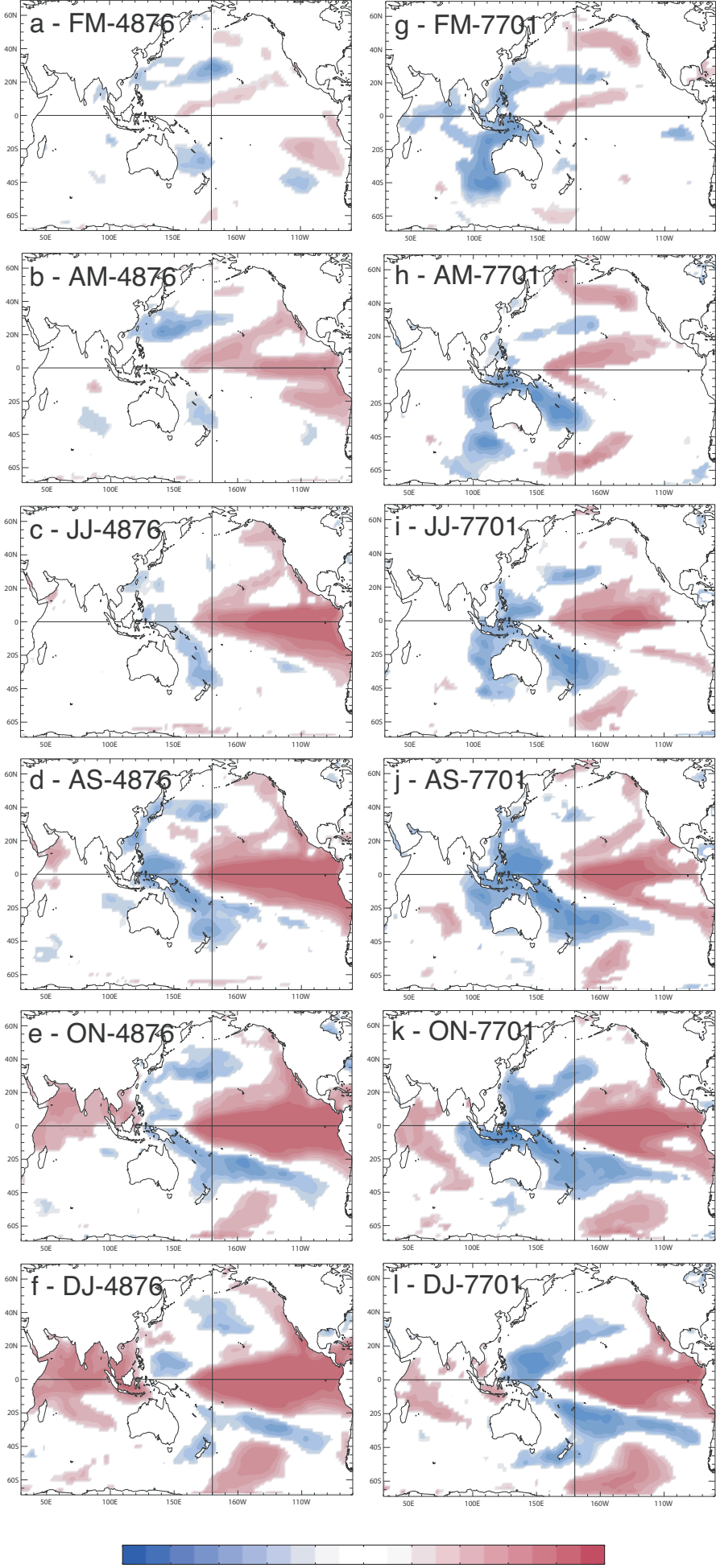
a - FM-4876
g - FM-7701
b - AM-4876
h - AM-7701
c - JJ-4876
i - JJ-7701
d - AS-4876
j - AS-7701
e - ON-4876
k - ON-7701
f - DJ-4876
l - DJ-7701
60N
40N
20N
0
20S
40S
60S
50E
100E
150E
160W
110W
-1.00
-0.80
-0.60
-0.40
-0.20
0.00
0.20
0.40
0.60
0.80
1.00
Correlation Nino34 SST (12-1) - SST

Figure 2

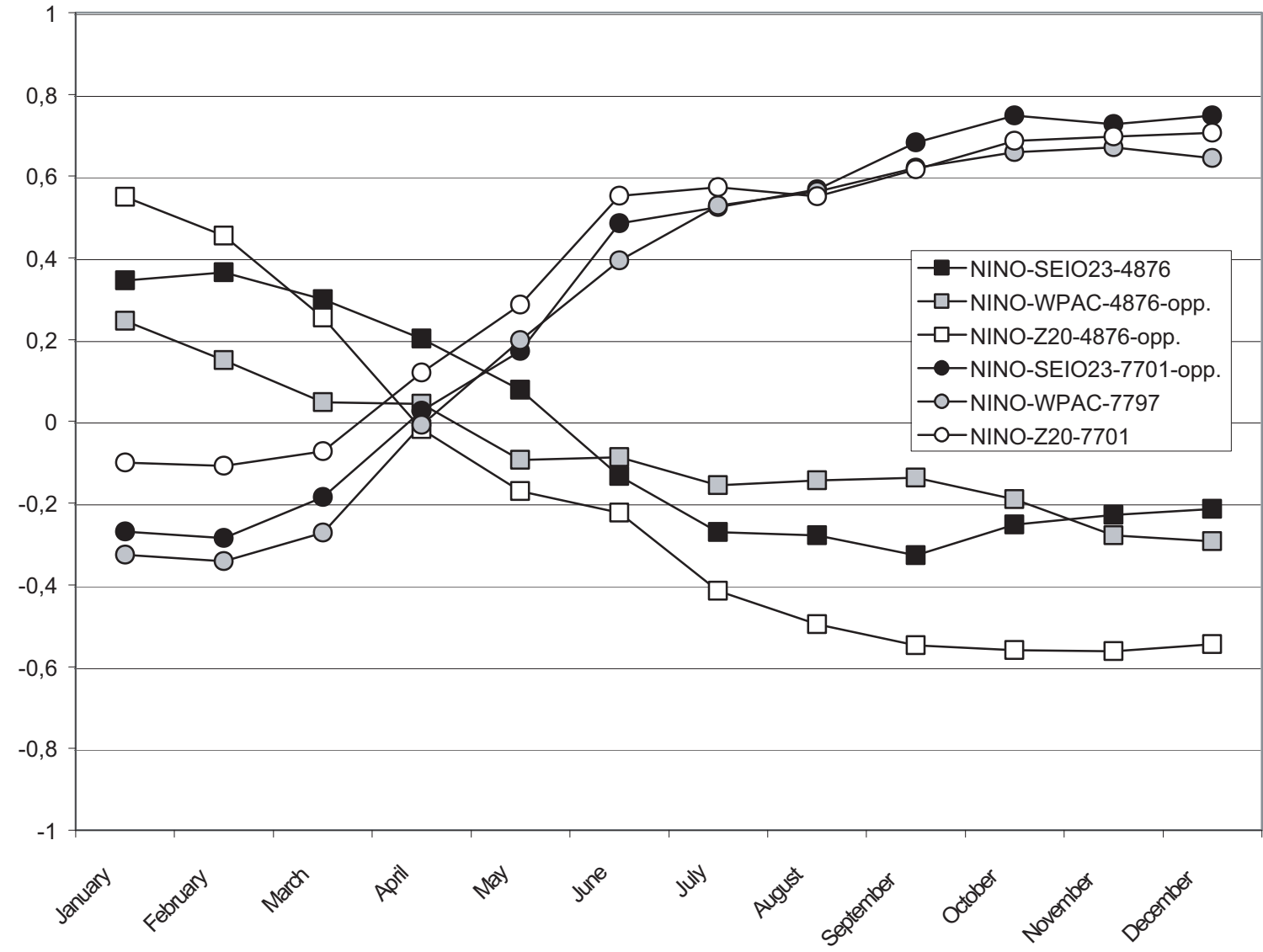
1
0,8
0,6
0,4
0,2
0
-0,2
-0,4
-0,6
-0,8
-1
January
February
March
April
May
June
July
August
September
October
November
December
NINO-SEIO23-4876
NINO-WPAC-4876-opp.
NINO-Z20-4876-opp.
NINO-SEIO23-7701-opp.
NINO-WPAC-7797
NINO-Z20-7701

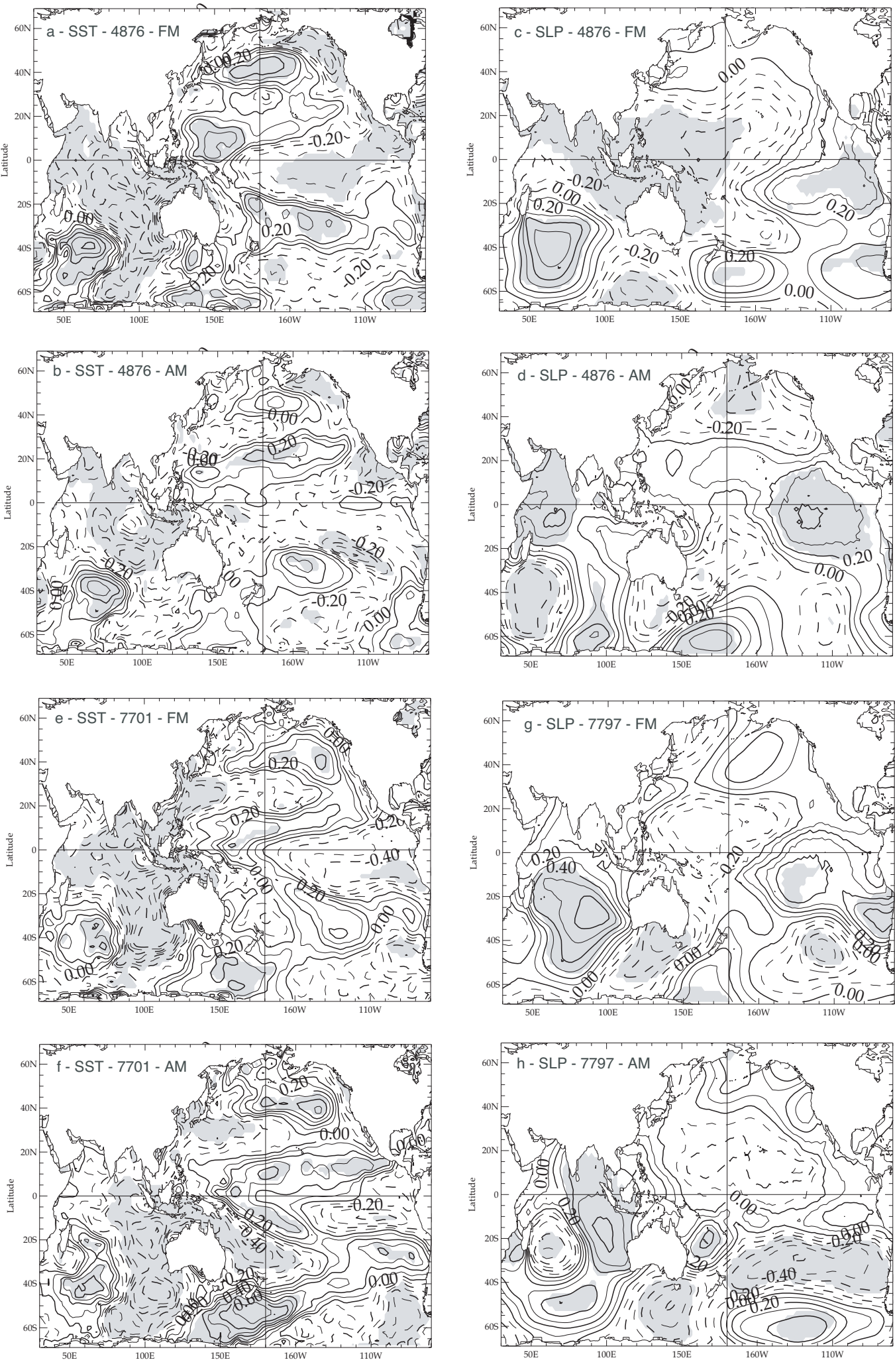

Figure 3 Correlation SEIO SST (2-3) - SST and SLP

Figure 4

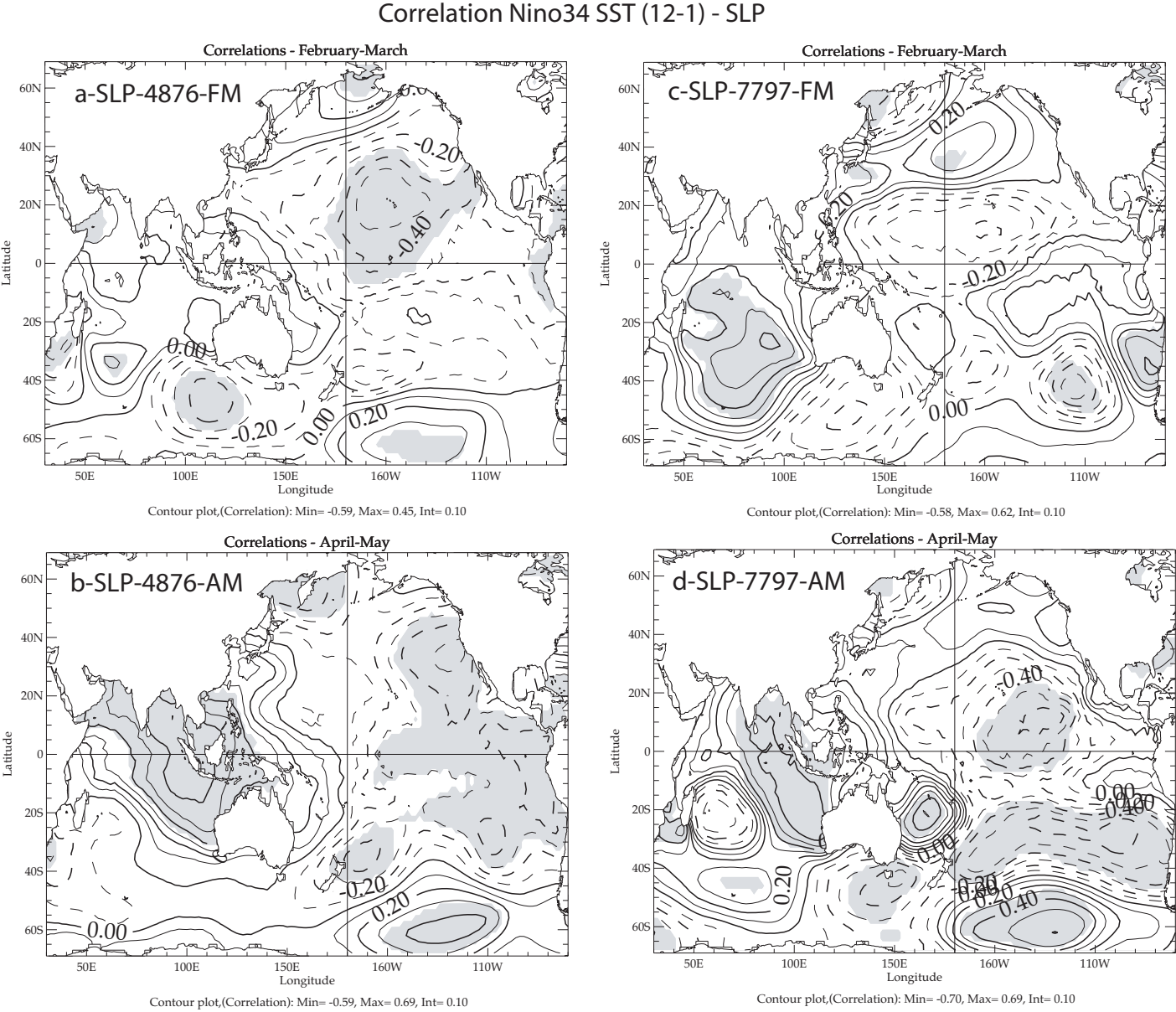
Correlation Nino34 SST (12-1) - SLP
Correlations - February-March
a-SLP-4876-FM
Latitude
Longitude
60N
40N
20N
0
20S
40S
60S
50E
100E
150E
160W
110W
-0.20
-0.40
0.00
0.20
Contour plot,(Correlation): Min= -0.59, Max= 0.45, Int= 0.10
Correlations - February-March
c-SLP-7797-FM
0.20
-0.20
0.00
Contour plot,(Correlation): Min= -0.58, Max= 0.62, Int= 0.10
Correlations - April-May
b-SLP-4876-AM
-0.20
0.20
0.00
Contour plot,(Correlation): Min= -0.59, Max= 0.69, Int= 0.10
Correlations - April-May
d-SLP-7797-AM
-0.40
0.00
0.20
0.40
Contour plot,(Correlation): Min= -0.70, Max= 0.69, Int= 0.10

Figure 5

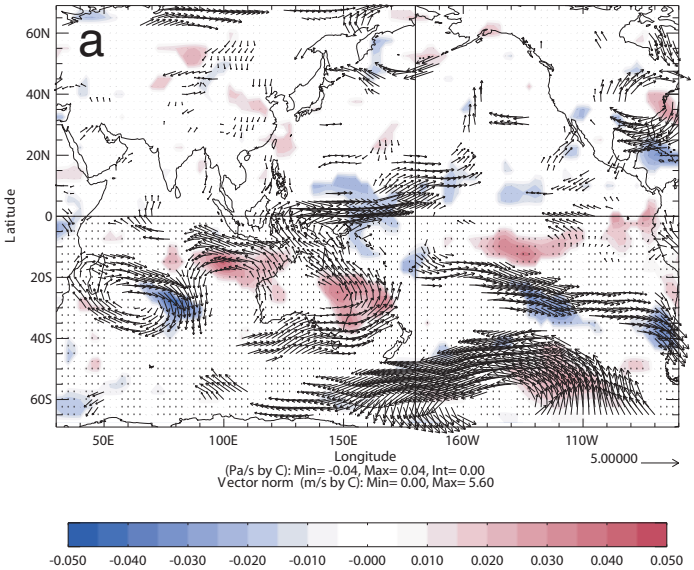
a
60N
40N
20N
0
20S
40S
60S
Latitude
50E
100E
150E
160W
110W
Longitude
5.00000
(Pa/s by C): Min= -0.04, Max= 0.04, Int= 0.00
Vector norm (m/s by C): Min= 0.00, Max= 5.60
-0.050 -0.040 -0.030 -0.020 -0.010 -0.000 0.010 0.020 0.030 0.040 0.050

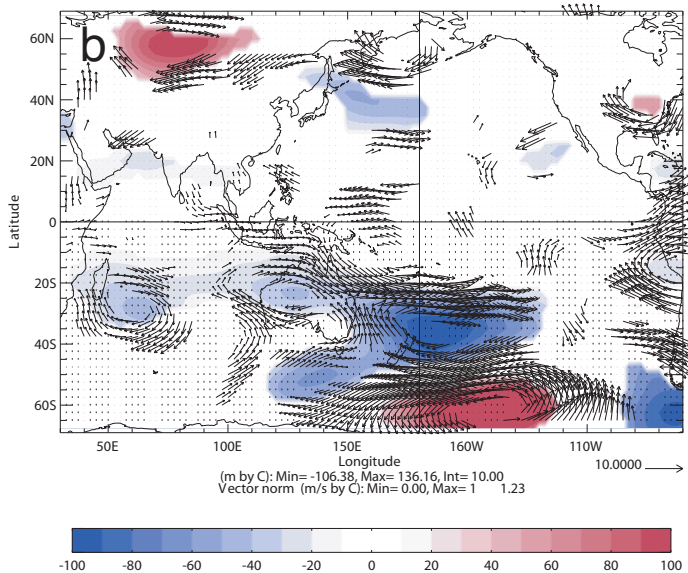
b
60N
40N
20N
0
20S
40S
60S
Latitude
50E
100E
150E
160W
110W
Longitude
10.0000
(m by C): Min= -106.38, Max= 136.16, Int= 10.00
Vector norm (m/s by C): Min= 0.00, Max= 1 1.23
-100 -80 -60 -40 -20 0 20 40 60 80 100

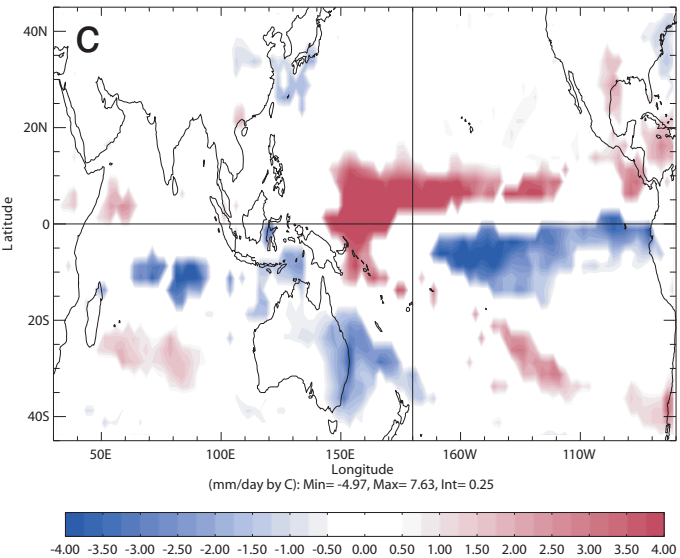
c
40N
20N
0
20S
40S
Latitude
50E
100E
150E
160W
110W
Longitude
(mm/day by C): Min= -4.97, Max= 7.63, Int= 0.25
-4.00 -3.50 -3.00 -2.50 -2.00 -1.50 -1.00 -0.50 0.00 0.50 1.00 1.50 2.00 2.50 3.00 3.50 4.00

Figure 6

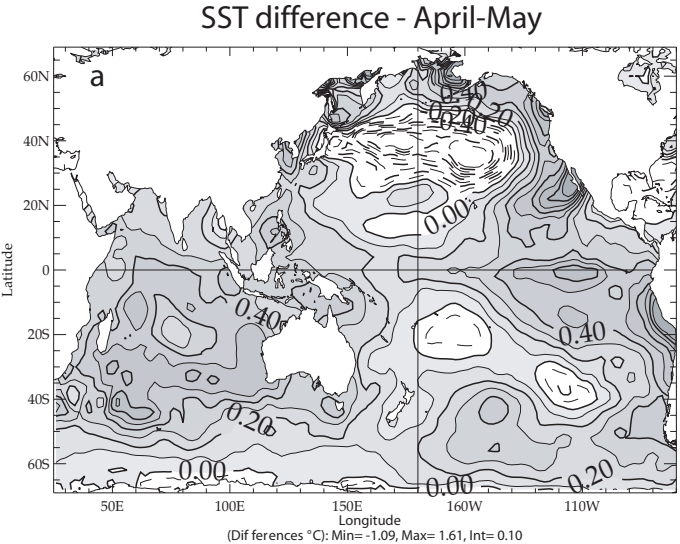
SST difference - April-May
a
60N
40N
20N
0
20S
40S
60S
Latitude
50E
100E
150E
160W
110W
Longitude
0.00
0.40
0.20
0.00
0.40
0.00
0.20
(Dif ferences °C): Min= -1.09, Max= 1.61, Int= 0.10

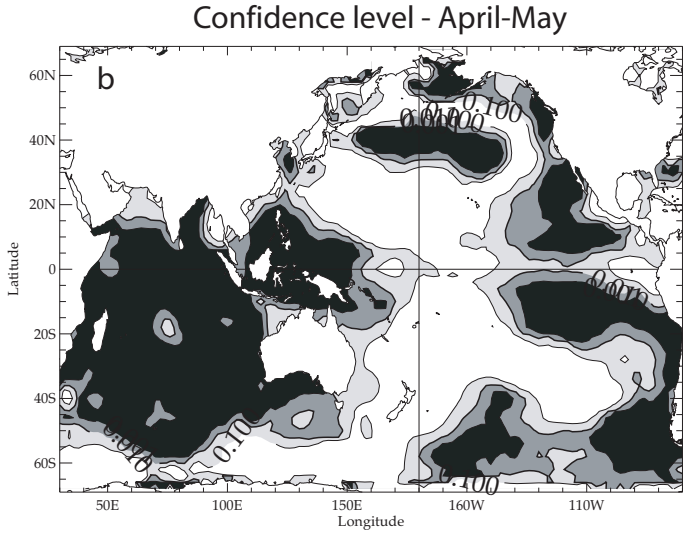
Confidence level - April-May
b
60N
40N
20N
0
20S
40S
60S
Latitude
50E
100E
150E
160W
110W
Longitude
0.100
0.010
0.001
0.10
0.001
0.100
Critical probabilities: 0.001(99.9%), 0.01(99%), 0.1(90%)

Figure 7

SVD analysis (SST with SLP) - 1948-1976 - ERSST and ERSLP

Homogeneous Vector (SST) - SVD Mode 1 (Squ.Cov.Fract. 57.7%)

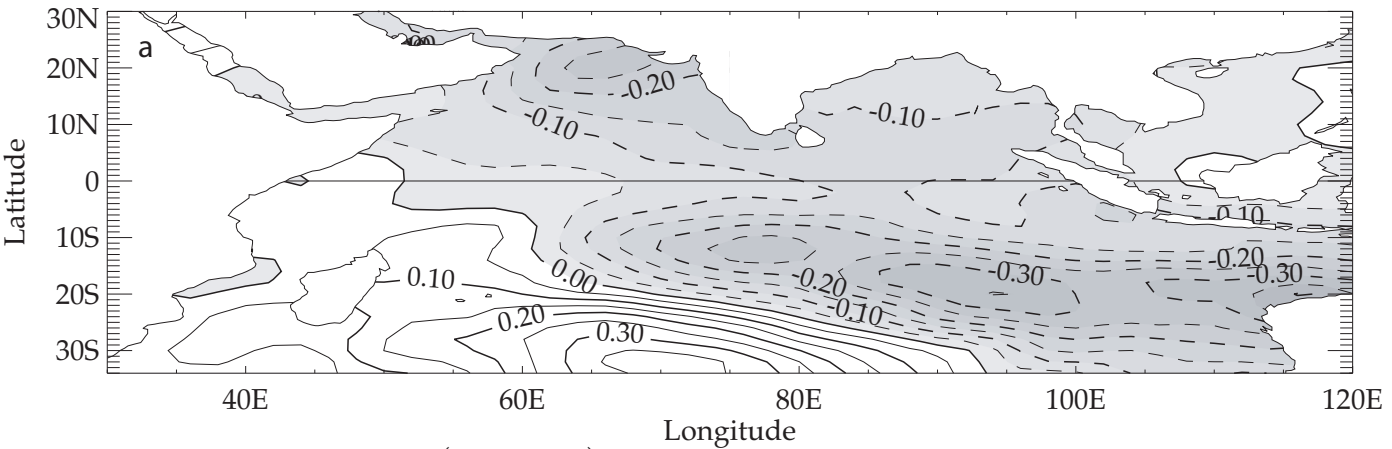

(covariance): Min= -0.40, Max= 0.38, Int= 0.05

Heterogeneous Vector (SLP) - SVD Mode 1 (Squ.Cov.Fract. 57.7%)

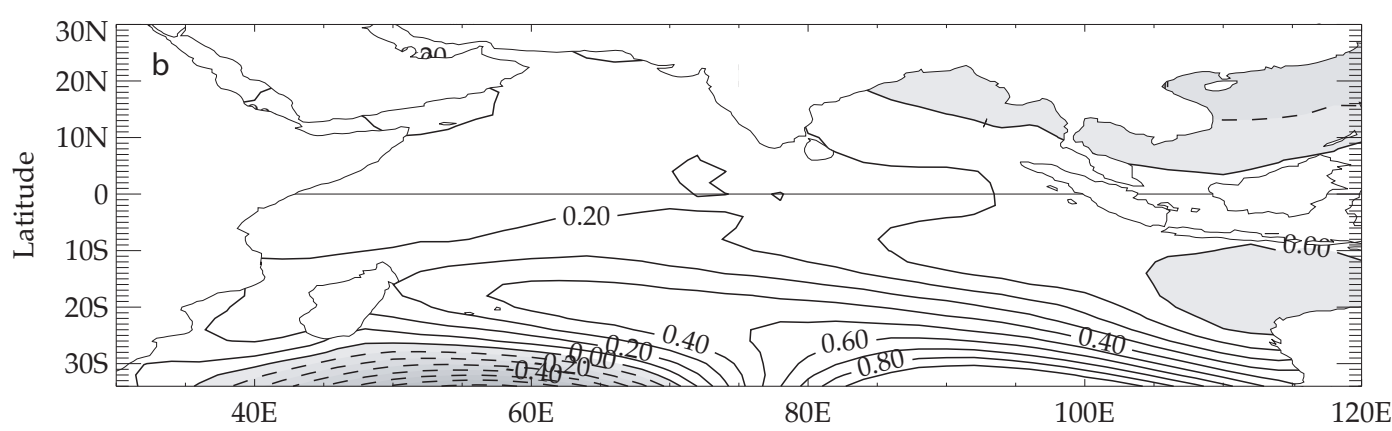

(covariance): Min= -0.73, Max= 1.22, Int= 0.10

Figure 8

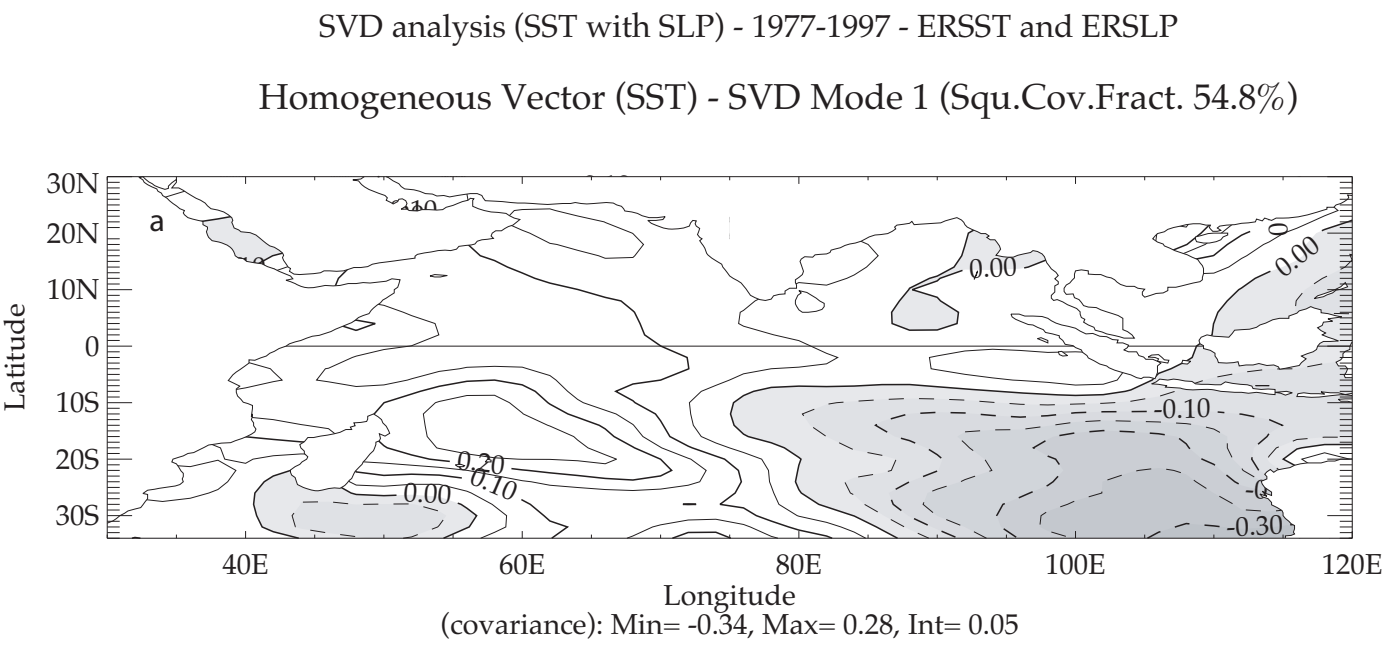
SVD analysis (SST with SLP) - 1977-1997 - ERSST and ERSLP
Homogeneous Vector (SST) - SVD Mode 1 (Squ.Cov.Fract. 54.8%)
a
30N
20N
10N
0
10S
20S
30S
Latitude
40E
60E
80E
100E
120E
Longitude
0.00
-0.10
0.20
0.10
0.00
-0.30
(covariance): Min= -0.34, Max= 0.28, Int= 0.05

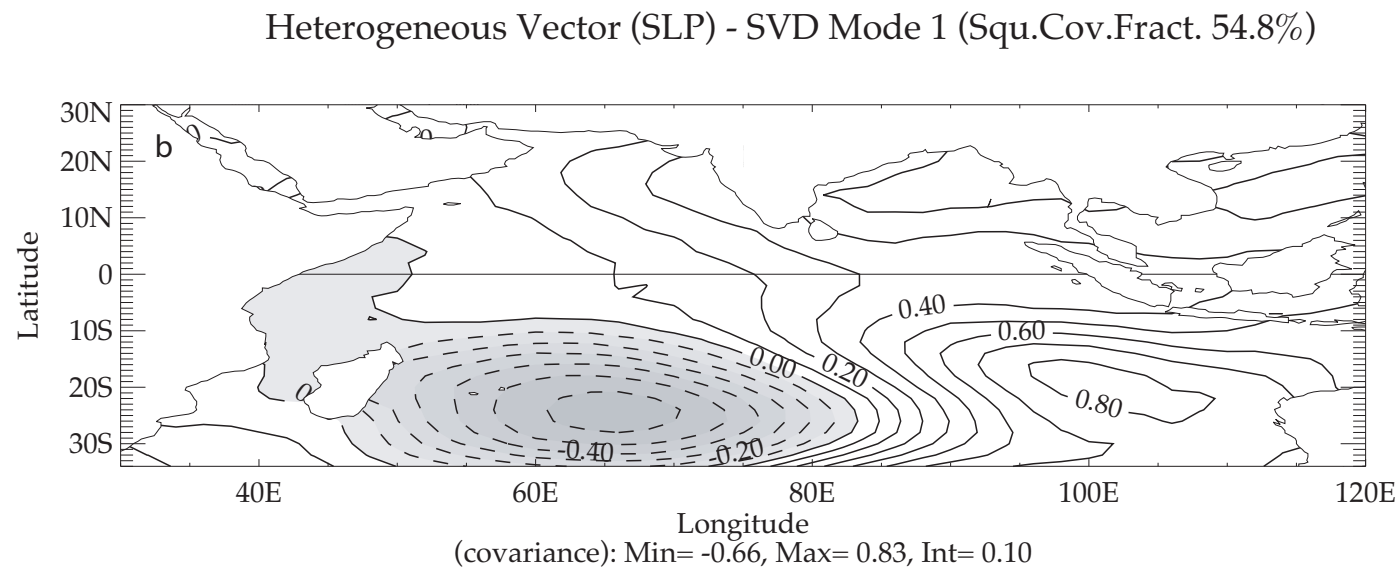
Heterogeneous Vector (SLP) - SVD Mode 1 (Squ.Cov.Fract. 54.8%)
b
30N
20N
10N
0
10S
20S
30S
Latitude
40E
60E
80E
100E
120E
Longitude
0.40
0.60
0.00
0.20
0.80
-0.40
-0.20
(covariance): Min= -0.66, Max= 0.83, Int= 0.10